



(Fe, Al)-bearing post-perovskite in the Earth's lower mantle



Zhu Mao^{a,b,c,*}, Jung-Fu Lin^a, Jing Yang^a, Hui Bian^{b,c}, Jin Liu^a, Heather C. Watson^d,
Shu Huang^e, Jiuhua Chen^e, Vitali B. Prakapenka^f, Yuming Xiao^g, Paul Chow^g

^a Department of Geological Sciences, Jackson School of Geosciences, The University of Texas at Austin, Austin, TX 78712, USA

^b Laboratory of Seismology and Physics of Earth's Interior, School of Earth and Planetary Sciences, University of Science and Technology of China, Hefei, Anhui 230026, China

^c National Geophysics Observatory at Mengcheng, Anhui 233500, China

^d Department of Earth and Environmental Science, Rensselaer Polytechnic Institute, Troy, NY 12180, USA

^e Department of Mechanical and Materials Engineering, Florida International University, Miami, FL 33172, USA

^f Center for Advanced Radiation Sources, University of Chicago, Chicago, IL 60637, USA

^g HPCAT, Geophysical Laboratory, Carnegie Institution of Washington, Argonne, IL 60439, USA

ARTICLE INFO

Article history:

Received 25 April 2014

Received in revised form 23 June 2014

Accepted 25 June 2014

Available online xxxx

Editor: J. Brodholt

Keywords:

(Fe, Al)-bearing post-perovskite
spin transition
equation of state
lower mantle
D'' layer

ABSTRACT

The combined effects of Fe and Al on the electronic spin and valence states as well as the equation of state (EoS) of post-perovskite have been investigated using synchrotron X-ray diffraction and Mössbauer spectroscopy in high-pressure diamond anvil cells. Two post-perovskite samples ($\text{Mg}_{0.6}\text{Fe}_{0.15}\text{Al}_{0.5}\text{Si}_{0.75}\text{O}_3$ and $\text{Mg}_{0.66}\text{Fe}_{0.13}\text{Al}_{0.28}\text{Si}_{0.86}\text{O}_3$) were synthesized at approximately 165 GPa and 2200–2500 K, and were subsequently investigated for these properties at 114–170 GPa and 300 K. Analyses of the high-pressure Mössbauer spectra show that Fe^{2+} and Fe^{3+} occupy the large bipolar prismatic sites in both of our samples and remain in the high-spin state at ~ 165 – 168 GPa and 300 K. Combining the Mössbauer results with the obtained pressure–volume relationship from X-ray diffraction, we have found that the unit cell volume of post-perovskite can be significantly affected by the spin and valence states of Fe and the Al substitution. $\text{Mg}_{0.6}\text{Fe}_{0.15}\text{Al}_{0.5}\text{Si}_{0.75}\text{O}_3$ -PPv with the predominantly high-spin Fe^{2+} ($\sim 95\%$) and a greater amount of Al has a unit cell volume similar to that of $\text{Mg}_{0.66}\text{Fe}_{0.13}\text{Al}_{0.28}\text{Si}_{0.86}\text{O}_3$ -PPv in which $\sim 65\%$ of Fe is in the high-spin Fe^{3+} state. Our results are used together with previous results regarding the EoS parameters in Fe-bearing perovskite and post-perovskite to model the density and bulk sound velocity variation between perovskite and post-perovskite in the D'' layer, in which the enrichment of Fe and Al can produce an increase in density but substantially reduce the bulk sound velocity across the phase transition. That is, the combined effect of Fe and Al leads to an anti-correlation between the enhanced density and the reduced bulk sound velocity at the pressure condition of the lowermost mantle. Our results indicate that (Fe, Al)-rich silicate post-perovskite existing in the D'' region would be shown as a relatively high-density and low-velocity region in deep-mantle seismic observations.

© 2014 Elsevier B.V. All rights reserved.

1. Introduction

The bottom 200–300 km of the lower mantle above the core–mantle boundary (CMB), which is typically referred as the D'' layer and characterized by a discontinuous increase in velocity, is one of the most seismically complex regions in the Earth (e.g. Garnero, 2000; Lay and Helmberger, 1983; van der Hilst et al., 2007). Various velocity anomalies, such as the ultra-low velocity zones (Garnero and Helmberger, 1995; Wen and Helmberger, 1998; Williams and Garnero, 1996), anomalous velocity gradient (e.g. He et al., 2006; Lay et al., 1998), velocity discontinuity (e.g. Sidorin et al., 1999; van der Hilst et al., 2007), and strong seismic velocity anisotropies (e.g. Lay et al., 1998; Panning and Romanowicz,

2004), have been identified in the region. In 2004, the discovery of the Mg-silicate perovskite (Pv) to post-perovskite (PPv) phase transition increased our understanding of the unusual characteristics of the D'' layer (Murakami et al., 2004; Oganov and Ono, 2004). In the last decade since its discovery, both experimental and theoretical studies have reported a wealth of exciting results pertaining to the physical properties of PPv, greatly contributing to our understanding of the structure, composition, and dynamic behavior of the lowermost mantle (e.g. Cobden et al., 2012; Dobson et al., 2013; Hirose, 2006; Lay et al., 2006; Mao et al., 2006; Shieh et al., 2006; Shim, 2008; van der Hilst et al., 2007; Zhang et al., 2013).

Of particular importance is the equation of state (EoS) of (Fe, Al)-PPv at relevant pressure–temperature–composition conditions of the D'' layer, which can provide crucial constraints on the density (ρ), elasticity, and bulk sound velocity (V_ϕ) of the

* Corresponding author.

lowermost mantle. However, experimental studies on the compositional effect, including the addition of Fe and Al, on the EoS of Mg-silicate PPv have so far been limited due to the challenging experimental pressure and temperature conditions along with the technical capability to reliably determine the spin and valence states of iron (Catalli et al., 2010a; Guignot et al., 2007; Lin et al., 2008; Mao et al., 2006; Nishio-Hamane and Yagi, 2009; Shieh et al., 2006). In Al-free PPv, previous studies have focused on the EoS of PPv with Fe content [Fe/(Fe + Mg)] up to 40% (Catalli et al., 2010a; Guignot et al., 2007; Mao et al., 2006; Shieh et al., 2006). Addition of Fe has been found to greatly increase the density of PPv, yet has a negligible effect on the isothermal bulk modulus (K_T) and V_ϕ when the amount of Fe is less than 10% (Catalli et al., 2010a; Guignot et al., 2007; Shieh et al., 2006) (for a recent review, please see Lin et al., 2013). Mao et al. (2006), on the other hand, has shown that the presence of 40% Fe can significantly increase the K_T by 39% at a pressure of 125 GPa and 300 K. Since there are no compression data for PPv with an Fe content between 10% and 40%, the question on how the substitution of Fe in PPv starts to affect its K_T remains open.

Studies on the net effect of Fe and Al on the EoS of PPv are even more scarce (Nishio-Hamane and Yagi, 2009; Shieh et al., 2011). Shieh et al. (2011) worked on the pressure–volume (P - V) relationship of (Fe, Al)-bearing PPv in the pyrope–almandine composition system, showing a linear increase in density with Fe content; however, the combined effect of Fe and Al on the K_T and V_ϕ was not addressed in Shieh et al. (2011) because they focused on the stability of Al-bearing PPv with a great amount of Fe. Studies by Nishio-Hamane and Yagi (2009) on the EoS of $\text{Mg}_{0.85}\text{Fe}_{0.15}\text{Al}_{0.15}\text{Si}_{0.85}\text{O}_3$ -PPv showed a great decrease in the K_T and V_ϕ because of the presence of the FeSiO_3 and FeAlO_3 components.

More interestingly, the D'' layer has been proposed to be chemically heterogeneous in previous studies (e.g. Buffett et al., 2000; Dobson and Brodholt, 2005; Mao et al., 2006; Williams and Garnero, 1996). Enrichment of Fe in the D'' layer may be caused by interaction between the lowermost mantle and the outer core or the subduction of slabs with mid-ocean ridge basalt (MORB) (e.g. Dobson and Brodholt, 2005; Knittle and Jeanloz, 1989, 1991; Mao et al., 2006; McNamara and Zhong, 2005; Otsuka and Karato, 2012). In addition, sinking slabs can deliver a great amount of Al to the lower mantle through the aluminous phase with the Ca-ferrite structure (Funamori et al., 2000; Hirose et al., 1999; Kesson et al., 1994). Therefore, experimental constraints on the combined effect for the enrichment of Fe and Al on the EoS of PPv would significantly enhance our understanding of the chemical heterogeneity and velocity anomalies in the Earth's D'' layer.

Previous studies on the spin and valence states of Fe in PPv have shown that Fe^{3+} in the bipolar prismatic sites (Mg) stays in the high spin (HS) state at lower mantle pressures, whereas it transforms into the low spin (LS) state in the octahedral sites (Catalli et al., 2010a). In Al-free PPv, theoretical calculations showed that Fe^{3+} enters PPv through the Fe^{3+} - Fe^{3+} coupled substitution (Zhang and Oganov, 2006). The spin transition of Fe has been known to significantly affect the EoS of candidate lower-mantle minerals (e.g. Catalli et al., 2011; Chang et al., 2013; Fei et al., 2007b; Komabayashi et al., 2010; Li et al., 2004; Lin et al., 2005, 2013; Mao et al., 2011a, 2011b). The HS to LS transition of Fe^{2+} in ferroperrichite and Fe^{3+} in perovskite have been observed to abruptly decrease the unit cell volume associated with an increase in density (Komabayashi et al., 2010; Lin et al., 2013; Mao et al., submitted for publication). Spin transition of Fe has also been shown to cause an anomalous softening in the elasticity and sound velocities (Crowhurst et al., 2008; Marquardt et al., 2009; Wentzcovitch et al., 2009; Wu et al., 2013).

The effect of Fe spin transition on the EoS of PPv has been explored recently (Catalli et al., 2010a). It has been shown that the presence of Fe^{2+} increases the volume of PPv while the presence of the LS Fe^{3+} does not produce an observable effect on the volume of PPv and thus effectively increases the density of PPv (Catalli et al., 2010a). Theoretical calculations further indicate that the addition of Al can enhance the substitution of Fe^{3+} into PPv through the Fe^{3+} - Al^{3+} coupled substitution (Yu et al., 2012). Metastable LS Fe^{3+} could be present in the octahedral sites at high pressure–temperature conditions (Caracas, 2010; Hsu et al., 2012). However, thus far, there is only one experimental study on the spin and valence states of Fe in (Fe, Al)-bearing PPv using X-ray emission spectroscopy (XES) which suggested the presence of LS Fe^{3+} in the octahedral sites (Fujino et al., 2013). We note that X-ray emission spectroscopic data alone cannot be used to distinguish different valence states of Fe^{2+} and Fe^{3+} , and that the disappearance of the $K\beta'$ satellite peak in XES spectra can also be a result of pressure-induced spectral broadening effect (Mao et al., 2014). As such, the spin and valence states of Fe in (Fe, Al)-bearing PPv and their potential effects on the EoS of PPv remain unclear.

Here we have conducted high-pressure synchrotron Mössbauer spectroscopy (SMS) and X-ray diffraction (XRD) experiments on PPv in two distinct compositions ($\text{Mg}_{0.60}\text{Fe}_{0.15}\text{Al}_{0.5}\text{Si}_{0.75}\text{O}_3$ and $\text{Mg}_{0.66}\text{Fe}_{0.13}\text{Al}_{0.28}\text{Si}_{0.86}\text{O}_3$) at pressures up to 170 GPa. We used SMS results to provide crucial constraints on the spin and valence states of Fe in PPv, while using our XRD to decipher the combined effects of Al and Fe on the EoS of PPv at lowermost-mantle pressures. These results are modeled using the Birch–Murnaghan (BM) EoS to understand the combined effect of Al and Fe, and then to understand the seismic profiles and potential chemical heterogeneity in the D'' region.

2. Experimental details

^{57}Fe -enriched glass, $\text{Mg}_{0.66}\text{Fe}_{0.13}\text{Al}_{0.28}\text{Si}_{0.86}\text{O}_3$ (labeled as 0.28Al-PPv13 hereafter), and single-crystal ^{57}Fe -enriched pyrope, $\text{Mg}_{0.60}\text{Fe}_{0.15}\text{Al}_{0.5}\text{Si}_{0.75}\text{O}_3$ (labeled as 0.5Al-PPv15 hereafter), were used as the starting samples for the syntheses of PPv, respectively. The glass sample was synthesized from the powders of MgO , $^{57}\text{Fe}_2\text{O}_3$, Al_2O_3 and SiO_2 mixed in the appropriate ratios, where the enrichment of ^{57}Fe in the samples was greater than 95%. The chemical composition of the starting glass has been determined using the electron microprobe analyses, and the starting pyrope crystal was examined using XRD and electron microprobe analyses to determine the crystal structure and chemical composition (Mao et al., 2014). The same batch of pyrope crystals was also studied using SMS to investigate the spin and valence states of Fe from ambient conditions to high pressures and temperatures (Mao et al., 2014).

The starting samples were polished down to approximately 10 μm in thickness and subsequently cut into pieces of 25 μm in diameter. The sample disk was sandwiched between two dried NaCl layers of approximately 5 μm in thickness which was used as the pressure medium, pressure calibrant and thermal insulator (Fei et al., 2007a). Each sample assemblage was loaded into a symmetric diamond cell equipped with a pair of beveled diamonds of 75/300 μm in culet size and a pre-indented Re gasket with a hole of 40 μm diameter and 25 μm thickness. Each loaded sample was directly compressed to ~ 160 GPa at 300 K, and then laser heated at 2200–2500 K for approximately 14 h to fully transform the starting material to PPv at GSECARS of the Advanced Photon Source (APS), Argonne National Laboratory (ANL). The synthesized PPv samples were confirmed by XRD.

SMS measurements for the PPv samples were performed at HP-CAT of the APS, ANL using an X-ray beam with a 2 meV energy

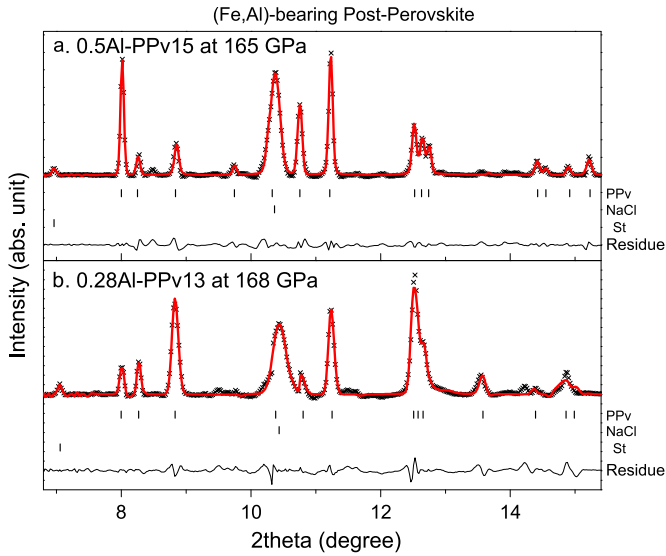


Fig. 1. Rietveld refinements of the representative X-ray diffraction patterns of the (Al, Fe)-bearing silicate PPv at high pressures. (a) 0.5Al-PPv15 with the chemical composition of $Mg_{0.6}Fe_{0.15}Al_{0.5}Si_{0.75}O_3$ at 165 GPa and 300 K; (b) 0.28Al-PPv13 with the chemical composition of $Mg_{0.66}Fe_{0.13}Si_{0.86}Al_{0.28}O_3$ at 168 GPa and 300 K. The full refinement results show that the synthesized samples were dominated by PPv (~96%) while a small amount of stishovite (St) (~4%) was also detected in each of the samples. In general, the X-ray diffraction patterns for both of the samples are consistent with each other. Refining the peaks above the 14° are much more difficult because they are relatively weaker. Since the PPv samples had to be synthesized at extreme pressure–temperature conditions for an extended period of time, these samples typically contained PPv grains of various sizes that contributed to the powder diffraction patterns, making it more difficult to refine the XRD patterns. Nevertheless, the X-ray diffraction patterns from both of the samples are in general consistent with each other.

resolution. We collected the SMS spectra for both of the samples with or without a $\sim 10 \mu\text{m}$ thick stainless steel foil with a natural ^{57}Fe abundance. The SMS spectrum of 0.5Al-PPv15 was collected at 165 GPa and 300 K, while the spectrum of 0.28Al-PPv13 was collected at 168 GPa and 300 K. The collection time for each spectrum was about 12 h.

After the SMS measurements, we also performed the XRD measurements for 0.5Al-PPv15 and 0.28Al-PPv13 in decompression at GSECARS of the APS, ANL, respectively. For 0.5Al-PPv15, the PPv structure was preserved to 127 GPa. Upon further decompression, the pressure suddenly dropped such that the 0.5Al-PPv15 sample lost the PPv structure and became amorphous. Similar to 0.5Al-PPv15, we only obtained the XRD pattern for 0.28Al-PPv13 down to 114 GPa. Further decompression also caused a sudden drop in pressure and a loss in the PPv structure.

3. Results

3.1. Rietveld refinements

Based on the full-profile Rietveld refinement results on the synthesized PPv at 165 GPa for 0.5Al-PPv15 and at 168 GPa for 0.28Al-PPv13, ~ 94 vol% of the synthesized phases were in the CaIrO_3 -type PPv structure (Fig. 1). The refinement cell parameters are: $a = 2.429(\pm 0.001)$, $b = 7.886(\pm 0.003)$, $c = 6.018(\pm 0.002)$ Å for 0.5Al-PPv15; $a = 2.426(\pm 0.001)$, $b = 7.942(\pm 0.003)$, $c = 6.021(\pm 0.002)$ Å for 0.28Al-PPv13. The refinements also show that the synthesized sample contained approximately 6 vol% stishovite coexisting with PPv. Since the Fe content in stishovite is likely negligible (Liu et al., 2007), the coexistence of stishovite with PPv should not affect the SMS results. The diffraction patterns for both of our (Fe, Al)-bearing PPv do not show the occurrence of the kinked structure, 2×1 type PPv ($P2_1/m$) (Fig. 1) that has been

previously reported to occur in Al-free PPv samples (Jackson et al., 2009; Mao et al., 2010). Comparing the composition of our samples with previous ones, it is possible that the presence of Al may limit the occurrence of the kinked structure. Detailed information on the Al substitution effect remains to be further investigated.

3.2. SMS analysis

The measured SMS spectra were analyzed using the CONUSS program (Sturhahn, 2000). For 0.5Al-PPv15, the spectrum can be suitably interpreted using a three-doublet model (Fig. 2 and Table 1). Doublet 1 with 48% abundance has an extremely high QS of $3.79(\pm 0.25)$ mm/s (Fig. 2 and Table 1). Compared to the QS of PPv and perovskite from literature results, doublet 1 is most likely to be the HS Fe^{2+} occupying the bipolar prismatic site (Lin et al., 2013; Yu et al., 2012) (Fig. 3). As shown in Lin et al. (2012), increasing pressure can greatly intensify the lattice distortion of Fe^{2+} in the bipolar prismatic sites, leading to a significant increase in the QS above 3.5 mm/s from 35 GPa (Lin et al., 2012) (Fig. 3). Since perovskite and PPv are structurally related, the extremely high QS in our PPv sample may also indicate a strong distortion of the Fe^{2+} sites. Doublet 2 with 47% abundance and QS of $2.40(\pm 0.25)$ mm/s has also been assigned to be the HS Fe^{2+} in the bipolar prismatic site (Lin et al., 2013; Yu et al., 2012) (Fig. 3). Considering the low QS value of $0.53(\pm 0.25)$ mm/s, the remaining 5% Fe in 0.5Al-PPv15 is assigned as the HS Fe^{3+} in the bipolar prismatic site, because the LS Fe^{3+} in the octahedral site would exhibit a higher QS of ~ 2 mm/s (Fig. 3) (Catalli et al., 2010a; Hsu et al., 2011; Lin et al., 2012; Mao et al., 2010; Yu et al., 2012).

For 0.28Al-PPv13, the doublet 1 also exhibits an extremely high QS of $4.03(\pm 0.25)$ mm/s. Based on the aforementioned discussion and comparison with the literature data for perovskite and PPv, we assign the doublet 1 as the HS Fe^{2+} in the bipolar prismatic site with strong lattice distortions (Fig. 3) (Lin et al., 2013; Yu et al., 2012). The doublet 2 with 13% occupancy has a QS of $1.62(\pm 0.25)$ mm/s, and the doublet 3 with 49% occupancy has a QS of $1.37(\pm 0.25)$ mm/s. Both of them are assigned as the HS Fe^{3+} in the bipolar prismatic site (Catalli et al., 2010a; Dyar et al., 2006; Lin et al., 2013; Yu et al., 2012) (Fig. 3). Based on the discussion above, we conclude that all of the Fe in 0.5Al-PPv15 and 0.28Al-PPv13 is in the HS state in the bipolar prismatic sites. Fe in 0.5Al-PPv15 is predominantly HS Fe^{2+} with a minor amount of HS Fe^{3+} , whereas more than 60% of the Fe in 0.28Al-PPv13 is the HS Fe^{3+} together with $\sim 40\%$ of Fe being the HS Fe^{2+} .

3.3. XRD analyses

XRD patterns of the PPv samples have been measured in decompression for each composition. For 0.5Al-PPv15, we have obtained the P - V relation between 125 and 168 GPa (Fig. 4). Because PPv is not pressure quenchable to ambient conditions, its volume at ambient conditions (V_0) is unknown. Considering the narrow pressure range in our experiments, we have used the modified third-order BM-EoS to model the P - V data in order to reduce the uncertainty for the derived EoS parameters (Sata et al., 2002):

$$P = \left\{ P_{02} - \frac{1}{2}(3K_{02} - 5P_{02}) \left[1 - \left(\frac{V}{V_{02}} \right)^{-2/3} \right] + \frac{9}{8}K_{02} \left(K'_{02} - 4 + \frac{35P_{02}}{9K_{02}} \right) \left[1 - \left(\frac{V}{V_{02}} \right)^{-2/3} \right]^2 \right\} \times \left(\frac{V}{V_{02}} \right)^{-5/3} \quad (1)$$

where P_{02} , K_{02} , and V_{02} are the pressure, bulk modulus, and unit cell volume at a reference pressure, respectively. The subscript 2

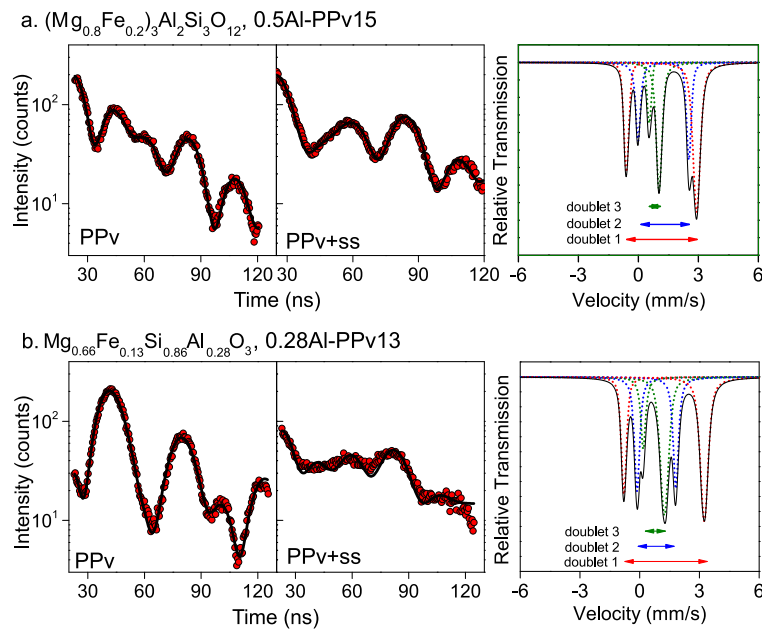


Fig. 2. Synchrotron Mössbauer spectra and modeled energy spectra of the (Al, Fe)-bearing silicate PPv at high pressures. Top panels: 0.5Al-PPv15 with the chemical composition of $(\text{Mg}_{0.8}\text{Fe}_{0.2})_3\text{Al}_2\text{Si}_3\text{O}_{12}$ at 165 GPa and 300 K; bottom panels: 0.28Al-PPv13 with the chemical composition of $\text{Mg}_{0.66}\text{Fe}_{0.13}\text{Si}_{0.86}\text{Al}_{0.28}\text{O}_3$ at 168 GPa and 300 K. Red circles: experimentally measured spectra; black lines: modeled results using CONUSS program (Sturhahn, 2000). Based on evaluation of the measured SMS spectra, the modeled energy spectra with assigned doublets for each PPv sample are shown on the right column. (For interpretation of the references to color in this figure legend, the reader is referred to the web version of this article.)

Table 1
Hyperfine parameters of PPv from SMS measurements.

Composition	Doublet	QS (mm/s)	IS (mm/s)	Abundance (%)
$\text{Mg}_{0.66}\text{Fe}_{0.13}\text{Al}_{0.28}\text{Si}_{0.86}\text{O}_3$ at 168 GPa	1	4.03	1.08	38
	2	1.37	0.29	49
	3	1.62	1	13
$\text{Mg}_{0.6}\text{Fe}_{0.15}\text{Al}_{0.5}\text{Si}_{0.75}\text{O}_3$ at 165 GPa	1	3.79	1	48
	2	2.40	1.35	47
	3	0.53	0.28	5

The uncertainties of QS and IS are ± 0.25 mm/s.

means that the reference is at high pressures. V is the measured unit cell volume, and K'_{02} is the pressure derivative of the bulk modulus. K'_{02} can be fixed as:

$$K'_{02} = 4 - \frac{35P_{02}}{9K_{02}} \quad (2)$$

In this model, Eq. (1) has been reduced to be the second order BM-EoS. Using the second order BM-EoS above, we have obtained $K_{02} = 726(\pm 30)$ GPa with $V_{02} = 115.3(\pm 0.3)$ \AA^3 at 165 GPa for 0.5Al-PPv15. The XRD patterns of 0.28Al-PPv13 were collected between 114 and 170 GPa during decompression (Fig. 4). Comparing to Al-free PPv, 0.28Al-PPv13 in this study exhibits greater compressibility (Fig. 4). The K_{02} of 0.28Al-PPv13 at 168 GPa is $760(\pm 30)$ GPa, together with $V_{02} = 115.8(\pm 0.3)$ \AA^3 at 168 GPa.

4. Discussion

4.1. Effect of Fe and Al on the volume of PPv

The SMS results from this study have provided valuable information on the spin and valence states of (Fe, Al)-bearing PPv, enabling us to better understand the compositional effect on the EoS of PPv. Based on the SMS results of 0.28Al-PPv13, Fe^{3+} and Al^{3+} enter the PPv structure through coupled-substitution, consistent with theoretical calculations (Zhang and Oganov, 2006).

The smaller Al^{3+} prefers to occupy the octahedral sites, which leads to the substitution of Fe^{3+} in the bipolar prismatic sites in the HS state. This is in contrast to the spin and valence states of Fe in Al-bearing perovskite in which the LS Fe^{3+} is also present in the octahedral sites at ~ 60 GPa together with Al (Catalli et al., 2011), indicating that the spin and valence states of Fe could be different in perovskite than PPv. According to the SMS results, the Fe^{3+} content is extremely low in 0.5Al-PPv15. About 95% of Fe in 0.5Al-PPv15 is HS Fe^{2+} , similar to that in the starting material. Although the self-oxidation of Fe^{2+} to form a certain amount of Fe^{3+} has been proposed to occur in PPv, the enrichment of Al in PPv may restrict this process and minimize the presence of Fe^{3+} (Jackson et al., 2009; Zhang and Oganov, 2006).

We also note that the volume of PPv is greatly affected by the different valence states of Fe and the amount of Al substitution. As mentioned above, Fe in 0.5Al-PPv15 is predominantly HS Fe^{2+} in the bipolar prismatic sites. The unit cell volume of 0.5Al-PPv15 should be greater than PPv with the same amount of Al and HS Fe^{3+} in the bipolar prismatic sites. However, due to the enrichment of Al, half of Al in 0.5Al-PPv15 will occupy the bipolar prismatic sites. The amount of Al present in the bipolar prismatic sites in 0.5Al-PPv15 is much greater than that in 0.28Al-PPv13, which can compensate for the volume difference between the HS Fe^{2+} and HS Fe^{3+} . As a result, 0.5Al-PPv15 with higher Al and HS Fe^{2+} contents has a unit cell volume similar to 0.28Al-PPv13 with lower Al and greater HS Fe^{3+} contents at the investigated pressure range (Fig. 4). We thus conclude that the unit cell volume of PPv is not only affected by the composition, but also by the valence and spin state of Fe.

4.2. Effect of Fe and Al on the density, K_T , and V_ϕ of PPv

We have compared our EoS parameters of PPv results to literature data in the pyrope–almandine (py–alm) composition system in order to understand the effect of Fe on the density, K_T , and V_ϕ of Al-enriched PPv at lowermost-mantle pressures and 300 K (Figs. 5 and 6). Addition of Fe causes a linear increase in the unit cell volume of PPv. The unit cell volume of Alm38–PPv

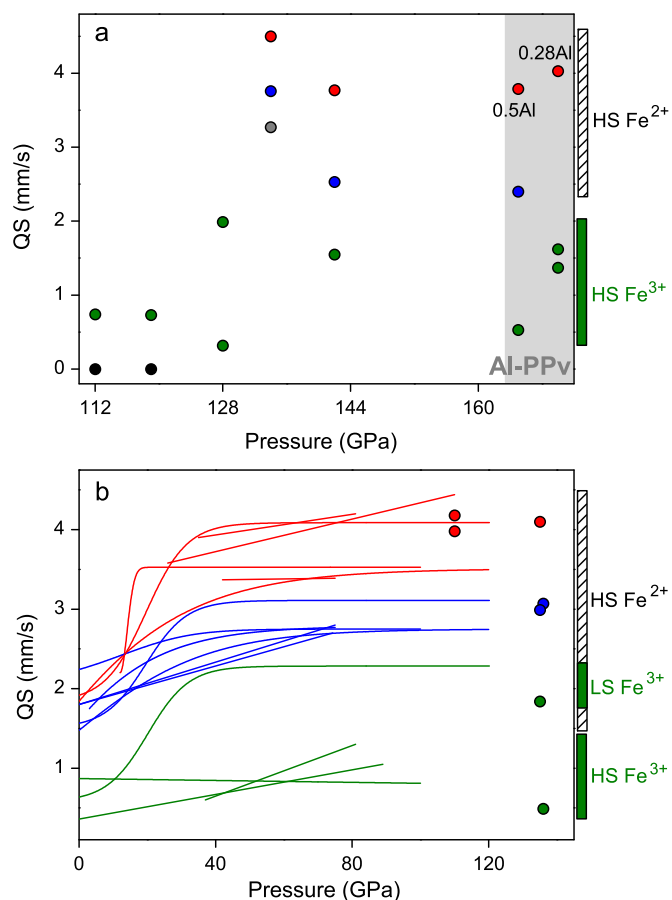


Fig. 3. Quadrupole splitting (QS) values of silicate PPv and perovskite at high pressures. (a) QS of PPv from literature and this study; (b) QS of perovskite from literature. In panel (a), red and blue circles: QS of Fe^{2+} occupying two different bipolar prismatic sites in PPv; green circles: QS of Fe^{3+} in PPv; black circles: QS of metallic iron (Jackson et al., 2009); grey circle: QS of unassigned site in PPv (Lin et al., 2008). Data for the QS of PPv are from literatures (Catalli et al., 2010a; Jackson et al., 2009; Lin et al., 2008; Mao et al., 2010) and this study. Due to the narrow stability pressure range of PPv in the lower mantle, the effect of pressure on the QS of PPv is not clear, which requires future Mössbauer studies over an extended pressure range. In panel (b), red and blue lines and circles: QS of Fe^{2+} occupying the large bipolar prismatic M1 and M2 sites in perovskite; green lines and circles: QS of Fe^{3+} in perovskite. Data for the QS of perovskite are from literatures (Catalli et al., 2010b; Jackson et al., 2005; Li et al., 2006; Lin et al., 2008, 2012; Mao et al., 2011b; McCammon et al., 2008; Narygina et al., 2010). The left dashed-vertical bar shows the range of QS for the HS Fe^{2+} , and the green-vertical bar shows the range of QS for the HS and LS Fe^{3+} . Uncertainties are not shown when they are smaller than symbols. (For interpretation of the references to color in this figure legend, the reader is referred to the web version of this article.)

in Shieh et al. (2011) is questionable and not used in the analyses here (Fig. 5). Alm38-PPv exhibits a much lower unit cell volume than our 0.5Al-PPv15 with 20% of Fe, but similar to that of MgSiO_3 -PPv and $\text{Mg}_3\text{Al}_2\text{Si}_3\text{O}_{12}$ -PPv at a given pressure (Fig. 5) (Guignot et al., 2007; Tateno et al., 2005). The problematic volume of Alm38-PPv in Shieh et al. (2011) could be caused by the presence of an Al-rich PPv phase during synthesis, leading to a change in composition. The effect of Fe content on the density, K_T , and V_ϕ of PPv in the py-alm system has been investigated at 130, 140 and 150 GPa, respectively (Fig. 6). In general, the density, K_T , and V_ϕ of PPv exhibit a positive dependence on the Fe content. Specifically, addition of Fe in PPv produces a linear increase in the density. The effect of Fe content on the K_T and V_ϕ of PPv is relatively weak when it is less than 54%. Above 54%, the K_T and V_ϕ of PPv are dramatically increased by Fe in the py-alm system.

To gain a more comprehensive understanding on the combined effect of Fe and Al, we have compared the density, K_T , and V_ϕ

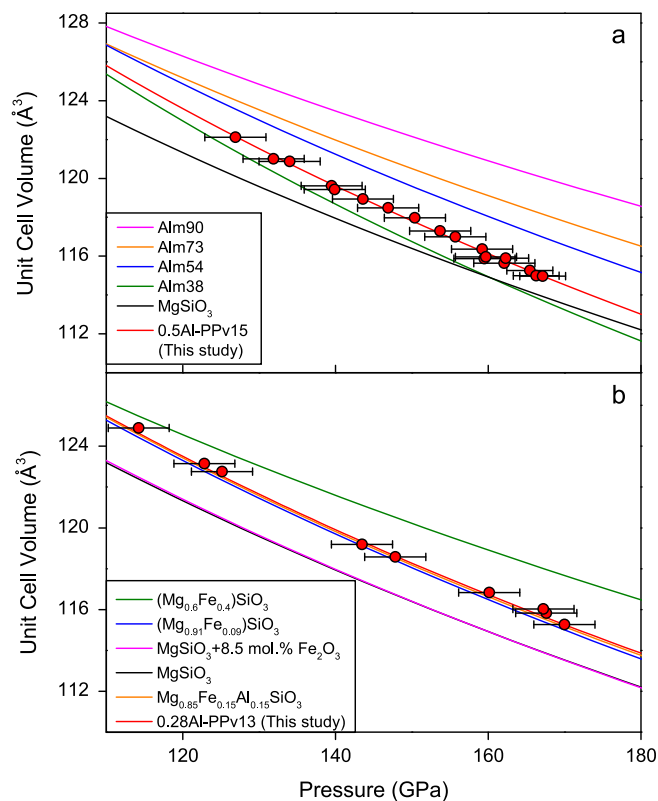


Fig. 4. Pressure–volume relations of (Fe, Al)-bearing PPv. (a) EoS of 0.5Al-PPv15 (red circles and lines). Black line: MgSiO_3 -PPv from Guignot et al. (2007); green, blue, orange and magenta lines are for PPv in Alm38, Alm54, Alm73 and Alm90 compositions from Shieh et al. (2011), respectively; (b) EoS of 0.28Al-PPv13 (red circles and lines). Black line: MgSiO_3 -PPv (Guignot et al., 2007); magenta line: PPv synthesized from $\text{MgSiO}_3 + 8.5 \text{ mol.}\% \text{ Fe}_2\text{O}_3$ (Catalli et al., 2010a); blue line: $(\text{Mg}_{0.91}\text{Fe}_{0.09})\text{SiO}_3$ -PPv (Shieh et al., 2006); green line: $(\text{Mg}_{0.6}\text{Fe}_{0.4})\text{SiO}_3$ -PPv (Mao et al., 2006). Errors are not shown when they are smaller than symbols. (For interpretation of the references to color in this figure legend, the reader is referred to the web version of this article.)

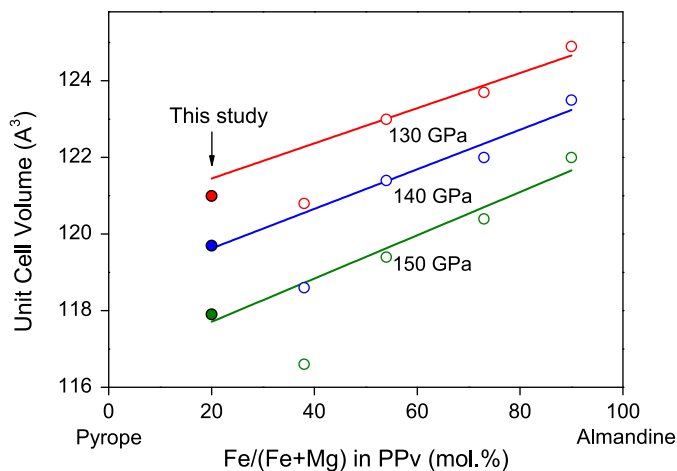


Fig. 5. Unit cell volumes of Al-bearing silicate PPv at high pressures. The results were derived from samples having chemical compositions in the pyrope-almandine series $[(\text{Mg}_x\text{Fe}_{1-x})_2\text{Si}_2\text{Al}_3\text{O}_{12}]$. Solid circles: 0.5Al-PPv15 (this study); open symbols: PPv in various compositions from Shieh et al. (2011); lines: linear relationship between the volume of PPv and Fe content in PPv at each given pressures. The data for Alm38-PPv from Shieh et al. (2011) were not used for the comparison because they obviously deviated from the linear relation between volume and Fe content.

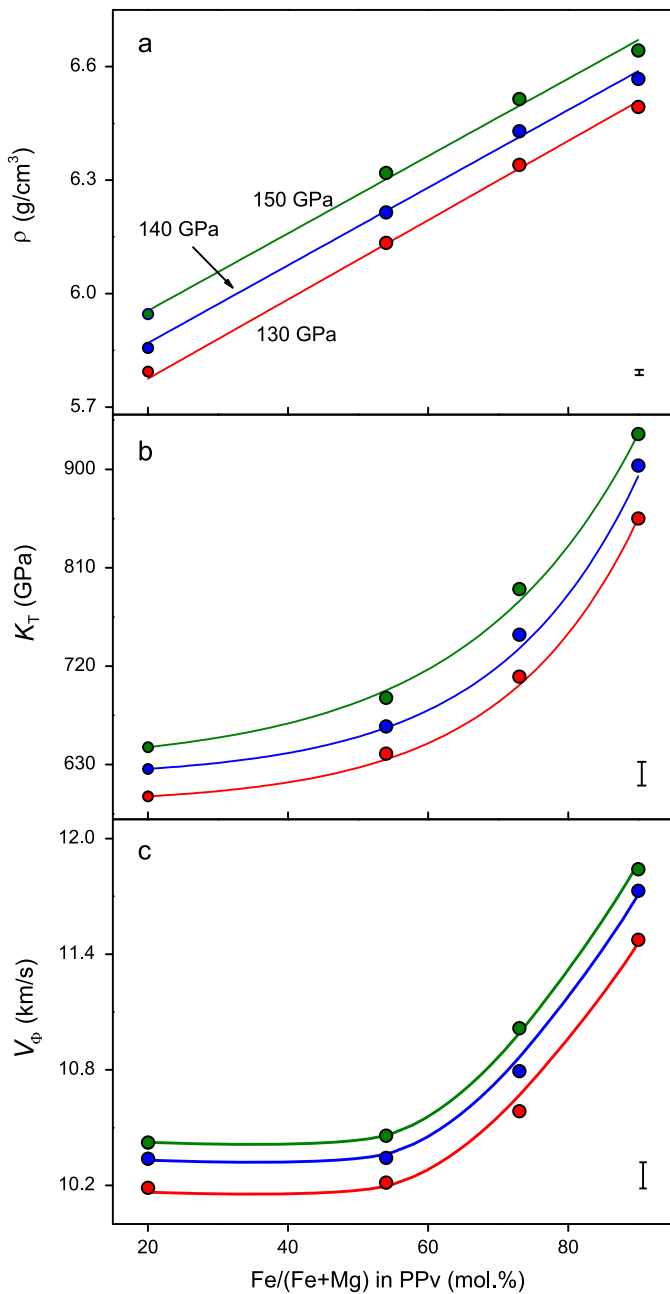


Fig. 6. Modeled density (ρ), bulk modulus (K_T), and bulk sound velocity (V_ϕ) of silicate PPv in pyrope–almandine composition at high pressures. Solid circles: calculated values based on the reported EoS from Shieh et al. (2011) and this study; red, blue and green colors are results at 130 GPa, 140 GPa and 150 GPa, respectively. The standard deviations of the volume and density are shown as $\pm 1\sigma$ at the bottom right corner of the figure. (For interpretation of the references to color in this figure legend, the reader is referred to the web version of this article.)

of our 0.5Al–PPv15 and 0.28Al–PPv13 to literature results in both of Al-free and Al-bearing PPv using MgSiO₃–PPv as a reference at lowermost-mantle pressures and 300 K (Fig. 7) (Guignot et al., 2007; Mao et al., 2006; Nishio-Hamane and Yagi, 2009; Shieh et al., 2011). When Al is absent in PPv, the density of (Mg, Fe)SiO₃–PPv increases with Fe content, similar to that shown in the py-alm composition system. (Fe, Al)-bearing PPv also exhibits a greater density than MgSiO₃–PPv. The presence of Al and HS Fe³⁺ in 0.28Al–PPv13 results in a $\sim 1(\pm 0.3)\%$ greater density than MgSiO₃–PPv at the CMB pressures; similar to the addition of 9% Fe in (Mg_{0.91}, Fe_{0.09})SiO₃–PPv. On the other hand, although the unit cell volumes of 0.5Al–PPv15 and 0.28Al–PPv13 are similar at

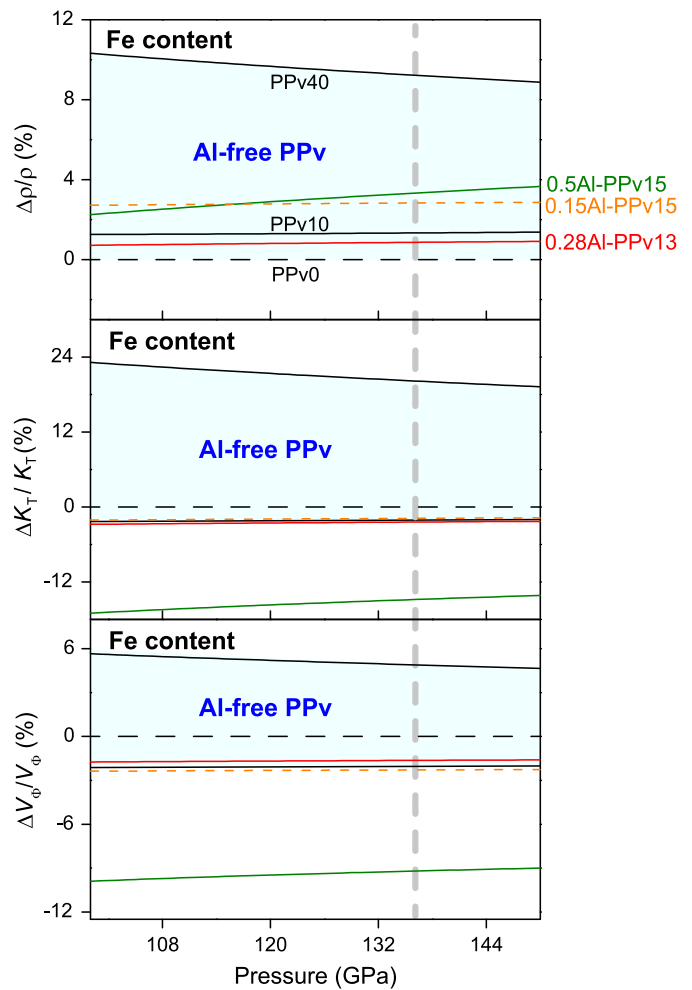


Fig. 7. Density (ρ), bulk modulus (K_T), and bulk sound velocity (V_ϕ) variation of (Al, Fe)-bearing PPv using MgSiO₃–PPv as the reference at pressures in the bottom lower mantle. $\Delta\rho/\rho$ (a), $\Delta K_T/K_T$ (b), and $\Delta V_\phi/V_\phi$ (c) represents the density, bulk modulus, and bulk sound velocity difference, respectively, between (Fe, Al)-bearing PPv and MgSiO₃–PPv. The blue area shows the effect of Fe content [0 (PPv0) to 40 mol% (PPv40)] on the density, bulk modulus, and bulk sound velocity of Al-free PPv (Mao et al., 2006; Shieh et al., 2006; Guignot et al., 2007). The red and green lines show the calculation results for 0.28Al–PPv13 and 0.5Al–PPv15, respectively, using results in this study. The orange short-dashed line is for 0.15Al–PPv15 from Nishio-Hamane and Yagi (2009). (For interpretation of the references to color in this figure legend, the reader is referred to the web version of this article.)

lowermost-mantle pressures, the enrichment of Al effectively increases the mass of 0.5Al–PPv15, leading to a greater density in 0.5Al–PPv15 than in 0.28Al–PPv13. At CMB pressures, 0.5Al–PPv15 has a density $\sim 3(\pm 0.4)\%$ greater than that of MgSiO₃–PPv. Nishio-Hamane and Yagi (2009) had reported the EoS parameters of (Mg_{0.85}Fe_{0.15})(Al_{0.15}Si_{0.85})O₃–PPv (0.15Al–PPv15), showing a density $2.8(\pm 0.3)\%$ greater than that of MgSiO₃–PPv at CMB pressures (Fig. 7). This is consistent with our results that the density of PPv exhibits a positive dependence on the Al and Fe content. However, it is difficult to directly compare our results to Nishio-Hamane and Yagi (2009) because of the different pressure calibrant used. More importantly, the spin and valance states of Fe are unknown in Nishio-Hamane and Yagi (2009), which have been shown to greatly influence the density of PPv at lowermost-mantle pressures.

The K_T and V_ϕ in Al-free PPv have been found to exhibit a negative dependence on the Fe content at up to 10% (Fig. 8), although Mao et al. (2006) has shown a great increase in the K_T and V_ϕ when the Fe content reaches 40%. The (Fe, Al)-bearing PPv has a lower K_T and V_ϕ than MgSiO₃–PPv, indicating a negative

Table 2
Unit cell parameters for PPv at high pressures.

Composition	P (GPa)	a (Å)	b (Å)	c (Å)	V (Å ³)	
Mg _{0.66} Fe _{0.13} Al _{0.28} Si _{0.86} O ₃	170(4)	2.423(2)	7.929(4)	5.999(4)	115.26(14)	
	168(4)	2.426(2)	7.939(4)	6.015(4)	115.83(14)	
	167(4)	2.426(2)	7.942(4)	6.021(4)	116.03(14)	
	158(4)	2.432(2)	7.962(4)	6.034(4)	116.83(14)	
	143(4)	2.447(2)	8.002(4)	6.056(4)	118.58(14)	
	141(4)	2.451(2)	8.024(4)	6.061(4)	119.20(14)	
	125(3)	2.466(4)	8.074(5)	6.166(6)	122.76(24)	
	123(3)	2.476(1)	8.080(5)	6.156(4)	123.15(12)	
	114(3)	2.487(2)	8.121(4)	6.183(3)	124.89(13)	
	Mg _{0.6} Fe _{0.15} Al _{0.5} Si _{0.75} O ₃	167(4)	2.426(1)	7.877(2)	6.018	114.97(06)
		166(4)	2.426(1)	7.878(2)	6.017	114.99(07)
165(4)		2.429(1)	7.886(4)	6.018(3)	115.26(09)	
162(4)		2.433(1)	7.901(4)	6.029(3)	115.90(10)	
162(4)		2.431(1)	7.895(4)	6.025(3)	115.63(09)	
160(4)		2.434(1)	7.901(4)	6.031(2)	115.96(08)	
160(4)		2.433(1)	7.898(4)	6.030(3)	115.87(10)	
159(4)		2.436(1)	7.918(3)	6.034(2)	116.36(08)	
156(4)		2.438(1)	7.947(3)	6.039(3)	116.99(08)	
154(4)		2.440(1)	7.949(3)	6.048(2)	117.29(08)	
150(4)		2.444(2)	7.970(4)	6.056(2)	117.97(12)	
147(4)		2.449(2)	7.959(4)	6.078(2)	118.48(12)	
144(4)		2.453(2)	7.980(4)	6.076(2)	118.94(12)	
140(4)		2.456(2)	7.989(5)	6.088(3)	119.43(14)	
139(4)		2.458(2)	7.989(4)	6.091(3)	119.61(13)	
134(4)		2.467(2)	8.026(5)	6.111(4)	121.00(15)	
132(3)		2.468(2)	8.035(5)	6.113(3)	121.23(14)	
127(3)	2.473(2)	8.059(5)	6.127(3)	122.12(14)		

Numbers in parentheses are one-standard deviation uncertainties in the last digit(s).

dependence on K_T and V_ϕ on the net content of Fe and Al. The K_T and V_ϕ of 0.28Al-PPv13 are 2.6(±4.3)% and 1.6(±1.5)% lower than those of MgSiO₃-PPv at CMB pressures, respectively. Addition of Al can enhance this reduction, leading to a 14.6(±4.9)% and 9.1(±2.0)% lower K_T and V_ϕ in 0.5Al-PPv15 than MgSiO₃-PPv at CMB pressures, respectively. The combined effect of Fe and Al on the K_T and V_ϕ of PPv is thus inverse to that on the density.

5. Geophysical implications

The density and velocity of candidate lower-mantle minerals at relevant pressure–temperature conditions are of two fundamental importance in constraining the composition, structure, and dynamic process of the region. Previous studies have pointed out that the perovskite to PPv phase transition can cause an increase in density yet a decrease in V_ϕ (Hirose, 2006; Nishio-Hamane and Yagi, 2009; Oganov and Ono, 2004; Wentzcovitch et al., 2006).

Using the EoS of 0.28Al-PPv13 and 0.5Al-PPv15 from this study together with previous results for (Fe, Al)-bearing perovskite, we have calculated the density and V_ϕ variation across the perovskite to PPv phase transition at the lowermost-mantle pressures and 300 K (Fig. 8) (Ballaran et al., 2012; Guignot et al., 2007; Lundin et al., 2008; Mao et al., 2006, 2011b, submitted for publication; Shieh et al., 2006). To reconcile different pressure calibrants used in the perovskite and PPv experiments (Mao et al., submitted for publication), we have used an internally consistent pressure scale from Fei et al. (2007a) to recalculate all pressures in our modeling. In this modeling, the volume percentage of perovskite in the lower mantle is assumed to be fixed at ~75% (Ringwood, 1975). Lower-mantle perovskite has been reported to undergo the HS to LS transition in Fe³⁺ (Hsu et al., 2011; Lin et al., 2012). The effect of Al and the Fe³⁺ spin transition on the density and V_ϕ of perovskite has been included in our modeling (Hsu et al., 2011; Lin et al., 2013; Mao et al., submitted for publication; Walter et al., 2006). Previous experimental studies have reported conflicting results on the partition of Fe between perovskite/PPv and ferropericline (Auzende et al., 2008; Kobayashi et al., 2005;

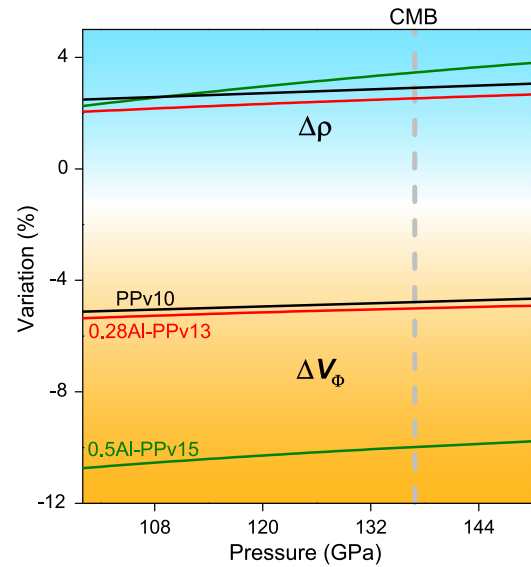


Fig. 8. Density (ρ) and bulk sound velocity variation (V_ϕ) for the perovskite to PPv phase transition. Black line: $\Delta\rho/\rho$ and $\Delta V_\phi/V_\phi$ between perovskite and PPv with 10% Fe; red line: $\Delta\rho/\rho$ and $\Delta V_\phi/V_\phi$ between perovskite and PPv with a 0.28Al-PPv13 composition; green line: $\Delta\rho/\rho$ and $\Delta V_\phi/V_\phi$ perovskite and PPv with a 0.5Al-PPv15 composition. (For interpretation of the references to color in this figure legend, the reader is referred to the web version of this article.)

Murakami et al., 2005; Sinmyo et al., 2008). Although previous experimental studies have shown that the spin transition of Fe may affect the partitioning of Fe between lower-mantle phases, all of the Fe in our PPv samples likely stays in the HS state because of the presence of Al, which should not affect the partitioning of Fe. To simplify the modeling, we have assumed that perovskite and PPv have the same Fe and Al content.

In the Al-free system, the presence of 10% Fe can produce a 2.9(±0.4)% increase in density and 4.8(±1.7)% decrease in V_ϕ at the CMB pressures due to the perovskite to PPv phase transi-

tion. For perovskite and PPv with the same composition as 0.28Al–PPv13, the phase transition will lead to a $2.5(\pm 0.4)\%$ increase in density and $5.0(\pm 1.7)\%$ decrease in V_{ϕ} , similar to the effect of 10% Fe. If the Fe and Al content in perovskite and PPv is as much as that shown in 0.5Al–PPv15, the density will be increased by $3.5(\pm 0.4)\%$, whereas the V_{ϕ} will decrease by $\sim 10(\pm 1.8)\%$ across the perovskite to PPv phase transition. The density and V_{ϕ} of the perovskite to PPv phase transition thus exhibit a strong dependence on the composition.

Previous experimental and theoretical studies have shown that the perovskite to PPv phase transition can cause an increase in the shear-wave velocity (Murakami et al., 2007a, 2007b). Together with the reduction in V_{ϕ} shown in our modeling, the shear-wave velocity and V_{ϕ} are anti-correlated, consistent with seismic observations (e.g. Masters et al., 2000; Su and Dziewonski, 1997). Most importantly, if some regions in the D'' layer have a MORB origin that is enriched in Fe and Al, the anomalies in V_{ϕ} across the phase transition will be enhanced (e.g. Dobson and Brodholt, 2005; Knittle and Jeanloz, 1989, 1991; McNamara and Zhong, 2005; Otsuka and Karato, 2012). Laterally, the enrichment of Fe and Al in PPv will also exhibit a seismic signature of a higher density but lower V_{ϕ} in the D'' layer. Such a compositional effect on V_{ϕ} will help us identify the chemical heterogeneity in the D'' layer. Since most studies used here were performed at high pressures and 300 K, future high pressure–temperature studies at relevant conditions of the D'' region are needed to provide a more comprehensive understanding of the compositional effect on the EoS parameters in the lowermost mantle region.

Acknowledgement

Z. Mao acknowledges support from China Thousand Young Talent Fellowship (KJ2080000016) and National Natural Science Foundation of China (41374092). J.F. Lin acknowledges support from the Geophysics Program and Instrumentation and Facility Program of the US National Science Foundation (EAR-0838221 and EAR-1053446). J.H. Chen acknowledges support from the Geophysics Program of the US National Science Foundation (EAR-1015509). Portions of this work were performed at GeoSoilEnviroCARS, Advanced Photon Source, Argonne National Laboratory. GSECARS was supported by the National Science Foundation (EAR-0622171) and U.S. Department of Energy (DE-FG02-94ER14466) under Contract No. DE-AC02-06CH11357. Portions of this work were performed at HPCAT (Sector 16) of the Advanced Photon Source (APS), Argonne National Laboratory. HPCAT is supported by CIW, CDAC, UNLV and LLNL through funding from DOE-NNSA, DOE-BES and NSF. APS is supported by DOE-BES, under Contract No. DE-AC02-06CH11357.

References

Auzende, A.L., Badro, J., Ryerson, F.J., Weber, P.K., Fallon, S.J., Addad, A., Siebert, J., Fiquet, G., 2008. Element partitioning between magnesium silicate perovskite and ferropericlase: new insights into bulk lower-mantle geochemistry. *Earth Planet. Sci. Lett.* 269, 164–174.

Ballaran, T.B., Kurnosov, A., Glazyrin, K., Frost, D.J., Merlini, M., Hanfland, M., Caracas, R., 2012. Effect of chemistry on the compressibility of silicate perovskite in the lower mantle. *Earth Planet. Sci. Lett.* 333, 181–190.

Buffett, B.A., Garnero, E.J., Jeanloz, R., 2000. Sediments at the top of Earth's core. *Science* 290, 1338–1342.

Caracas, R., 2010. Spin and structural transitions in AlFeO_3 and FeAlO_3 perovskite and post-perovskite. *Phys. Earth Planet. Inter.* 182, 10–17.

Catalli, K., Shim, S.H., Prakapenka, V.B., Zhao, J., Sturhahn, W., 2010a. X-ray diffraction and Mossbauer spectroscopy of Fe^{3+} -bearing Mg-silicate post-perovskite at 128–138 GPa. *Am. Mineral.* 95, 418–421. <http://dx.doi.org/10.2138/Am.2010.3352>.

Catalli, K., Shim, S.H., Prakapenka, V.B., Zhao, J.Y., Sturhahn, W., Chow, P., Xiao, Y.M., Liu, H.Z., Cynn, H., Evans, W.J., 2010b. Spin state of ferric iron in MgSiO_3 perovskite and its effect on elastic properties. *Earth Planet. Sci. Lett.* 289, 68–75.

Catalli, K., Shim, S.H., Dera, P., Prakapenka, V.B., Zhao, J.Y., Sturhahn, W., Chow, P., Xiao, Y.M., Cynn, H., Evans, W.J., 2011. Effects of the Fe^{3+} spin transition on the properties of aluminous perovskite–New insights for lower-mantle seismic heterogeneities. *Earth Planet. Sci. Lett.* 310, 293–302.

Chang, Y.Y., Jacobsen, S.D., Lin, J.F., Bina, C.R., Thomas, S.M., Wu, J.J., Shen, G.Y., Xiao, Y.M., Chow, P., Frost, D.J., McCammon, C.A., Dera, P., 2013. Spin transition of Fe^{3+} in Al-bearing phase D: an alternative explanation for small-scale seismic scatterers in the mid-lower mantle. *Earth Planet. Sci. Lett.* 382, 1–9.

Cobden, L., Mosca, I., Trampert, J., Ritsema, J., 2012. On the likelihood of post-perovskite near the core–mantle boundary: a statistical interpretation of seismic observations. *Phys. Earth Planet. Inter.* 210, 21–35.

Crowhurst, J.C., Brown, J.M., Goncharov, A.F., Jacobsen, S.D., 2008. Elasticity of $(\text{Mg,Fe})\text{O}$ through the spin transition of iron in the lower mantle. *Science* 319, 451–453.

Dobson, D.P., Brodholt, J.P., 2005. Subducted banded iron formations as a source of ultralow-velocity zones at the core–mantle boundary. *Nature* 434, 371–374.

Dobson, D.P., Miyajima, N., Nestola, F., Alvaro, M., Casati, N., Liebske, C., Wood, I.G., Walker, A.M., 2013. Strong inheritance of texture between perovskite and post-perovskite in the D'' layer. *Nat. Geosci.* 6, 575–578.

Dyar, M.D., Agresti, D.G., Schaefer, M.W., Grant, C.A., Sklute, E.C., 2006. Mössbauer spectroscopy of earth and planetary materials. *Annu. Rev. Earth Planet. Sci.* 34, 83–125.

Fei, Y.W., Ricolleau, A., Frank, M., Mibe, K., Shen, G.Y., Prakapenka, V., 2007a. Toward an internally consistent pressure scale. *Proc. Natl. Acad. Sci. USA* 104, 9182–9186.

Fei, Y.W., Zhang, L., Corgne, A., Watson, H., Ricolleau, A., Meng, Y., Prakapenka, V., 2007b. Spin transition and equations of state of $(\text{Mg,Fe})\text{O}$ solid solutions. *Geophys. Res. Lett.* 34. <http://dx.doi.org/10.1029/2007gl090712>.

Fujino, K., Nishio-Hamane, D., Kuwayama, Y., Sata, N., Murakami, S., Whitaker, M., Shinozaki, A., Ohfuji, H., Kojima, Y., Irifune, T., Hiraoka, N., Ishii, H., Tsuei, K.D., 2013. Spin transition and substitution of Fe^{3+} in Al-bearing post-Mg-perovskite. *Phys. Earth Planet. Inter.* 217, 31–35.

Funamori, N., Jeanloz, R., Miyajima, N., Fujino, K., 2000. Mineral assemblages of basalt in the lower mantle. *J. Geophys. Res.* 105, 26037–26043.

Garnero, E.J., 2000. Heterogeneity of the lowermost mantle. *Annu. Rev. Earth Planet. Sci.* 28, 509–537.

Garnero, E.J., Helmberger, D.V., 1995. A very slow basal layer underlying large-scale low-velocity anomalies in the lower mantle beneath the Pacific – evidence from core phases. *Phys. Earth Planet. Inter.* 91, 161–176.

Guignot, N., Andraud, D., Morard, G., Bolfan-Casanova, N., Mezouar, M., 2007. Thermoelastic properties of post-perovskite phase MgSiO_3 determined experimentally at core–mantle boundary P–T conditions. *Earth Planet. Sci. Lett.* 256, 162–168.

He, Y.M., Wen, L.X., Zheng, T.Y., 2006. Geographic boundary and shear wave velocity structure of the “Pacific anomaly” near the core–mantle boundary beneath western Pacific. *Earth Planet. Sci. Lett.* 244, 302–314.

Hirose, K., 2006. Postperovskite phase transition and its geophysical implications. *Rev. Geophys.* 44. <http://dx.doi.org/10.1029/2005rg000186>.

Hirose, K., Fei, Y.W., Ma, Y.Z., Mao, H.K., 1999. The fate of subducted basaltic crust in the Earth's lower mantle. *Nature* 397, 53–56.

Hsu, H., Blaha, P., Cococcioni, M., Wentzcovitch, R.M., 2011. Spin-state crossover and hyperfine interactions of ferric iron in MgSiO_3 perovskite. *Phys. Rev. Lett.* 106. <http://dx.doi.org/10.1103/PhysRevLett.106.118501>.

Hsu, H., Yu, Y.G., Wentzcovitch, R.M., 2012. Spin crossover of iron in aluminous MgSiO_3 perovskite and post-perovskite. *Earth Planet. Sci. Lett.* 359–360, 34–39.

Jackson, J.M., Sturhahn, W., Shen, G.Y., Zhao, J.Y., Hu, M.Y., Errandonea, D., Bass, J.D., Fei, Y.W., 2005. A synchrotron Mössbauer spectroscopy study of $(\text{Mg,Fe})\text{SiO}_3$ perovskite up to 120 GPa. *Am. Mineral.* 90, 199–205.

Jackson, J.M., Sturhahn, W., Tschauer, O., Lerche, M., Fei, Y.W., 2009. Behavior of iron in $(\text{Mg,Fe})\text{SiO}_3$ post-perovskite assemblages at Mbar pressures. *Geophys. Res. Lett.* 36. <http://dx.doi.org/10.1029/2009gl037815>.

Kesson, S.E., Fitz Gerald, J.D., Shelley, J.M.G., 1994. Mineral chemistry and density subducted basaltic crust at lower-mantle pressures. *Nature* 372, 767–769.

Knittle, E., Jeanloz, R., 1989. Simulating the core–mantle boundary – an experimental-study of high-pressure reactions between silicates and liquid–Iron. *Geophys. Res. Lett.* 16, 609–612.

Knittle, E., Jeanloz, R., 1991. Earth's core–mantle boundary – results of experiments at high-pressures and temperatures. *Science* 251, 1438–1443.

Kobayashi, Y., Kondo, T., Ohtani, E., Hirao, N., Miyajima, N., Yagi, T., Nagase, T., Kikegawa, T., 2005. Fe–Mg partitioning between $(\text{Mg,Fe})\text{SiO}_3$ post-perovskite, perovskite, and magnesiowüstite in the Earth's lower mantle. *Geophys. Res. Lett.* 32. <http://dx.doi.org/10.1029/2005gl023257>.

Komabayashi, T., Hirose, K., Nagaya, Y., Sugimura, E., Ohishi, Y., 2010. High-temperature compression of ferropericlase and the effect of temperature on iron spin transition. *Earth Planet. Sci. Lett.* 297, 691–699.

Lay, T., Helmberger, D.V., 1983. A lower mantle S-wave triplication and the shear velocity structure of D''. *Geophys. J. R. Astron. Soc.* 75, 799–837.

Lay, T., Hernlund, J., Garnero, E.J., Thorne, M.S., 2006. A post-perovskite lens and D'' heat flux beneath the central Pacific. *Science* 314, 1272–1276.

Lay, T., Williams, Q., Garnero, E.J., 1998. The core–mantle boundary layer and deep earth dynamics. *Nature* 392, 461–468.

- Li, J., Struzhkin, V.V., Mao, H.K., Shu, J.F., Hemley, R.J., Fei, Y.W., Mysen, B., Dera, P., Prakapenka, V., Shen, G.Y., 2004. Electronic spin state of iron in lower mantle perovskite. *Proc. Natl. Acad. Sci. USA* 101, 14027–14030.
- Li, J., Sturhahn, W., Jackson, J.M., Struzhkin, V.V., Lin, J.F., Zhao, J., Mao, H.K., Shen, G., 2006. Pressure effect on the electronic structure of iron in (Mg,Fe)(Si,Al)O₃ perovskite: a combined synchrotron Mössbauer and X-ray emission spectroscopy study up to 100 GPa. *Phys. Chem. Miner.* 33, 575–585.
- Lin, J.F., Alp, E.E., Mao, Z., Inoue, T., McCammon, C., Xia, Y.M., Chow, P., Zhao, J.Y., 2012. Electronic spin states of ferric and ferrous iron in the lower-mantle silicate perovskite. *Am. Mineral.* 97, 592–597.
- Lin, J.F., Speziale, S., Mao, Z., Marquardt, H., 2013. Effects of the electronic spin transitions of iron in lower-mantle minerals: implications to deep-mantle geophysics and geochemistry. *Rev. Geophys.* 51, 2012RG000414.
- Lin, J.F., Struzhkin, V.V., Jacobsen, S.D., Hu, M.Y., Chow, P., Kung, J., Liu, H.Z., Mao, H.K., Hemley, R.J., 2005. Spin transition of iron in magnesiowüstite in the Earth's lower mantle. *Nature* 436, 377–380.
- Lin, J.F., Watson, H., Vanko, G., Alp, E.E., Prakapenka, V.B., Dera, P., Struzhkin, V.V., Kubo, A., Zhao, J.Y., McCammon, C., Evans, W.J., 2008. Intermediate-spin ferrous iron in lowermost mantle post-perovskite and perovskite. *Nat. Geosci.* 1, 688–691.
- Liu, L., Zhang, J.F., Green, H.W., Jin, Z.M., Bozhilov, K.N., 2007. Evidence of former stishovite in metamorphosed sediments, implying subduction to >350 km. *Earth Planet. Sci. Lett.* 263, 180–191.
- Lundin, S., Catalli, K., Santillan, J., Shim, S.H., Prakapenka, V.B., Kunz, M., Meng, Y., 2008. Effect of Fe on the equation of state of mantle silicate perovskite over 1 Mbar. *Phys. Earth Planet. Inter.* 168, 97–102.
- Mao, W.L., Mao, H.K., Sturhahn, W., Zhao, J.Y., Prakapenka, V.B., Meng, Y., Shu, J.F., Fei, Y.W., Hemley, R.J., 2006. Iron-rich post-perovskite and the origin of ultralow-velocity zones. *Science* 312, 564–565.
- Mao, Z., Lin, J.F., Jacobs, C., Watson, H.C., Xiao, Y., Chow, P., Alp, E.E., Prakapenka, V.B., 2010. Electronic spin and valence states of Fe in CaIrO₃-type silicate post-perovskite in the Earth's lowermost mantle. *Geophys. Res. Lett.* 37. <http://dx.doi.org/10.1029/2010gl045021>.
- Mao, Z., Lin, J.F., Liu, J., Prakapenka, V.B., 2011a. Thermal equation of state of lower-mantle ferropericlase across the spin crossover. *Geophys. Res. Lett.* 38. <http://dx.doi.org/10.1029/2011gl049915>.
- Mao, Z., Lin, J.F., Scott, H.P., Watson, H.C., Prakapenka, V.B., Xiao, Y., Chow, P., McCammon, C., 2011b. Iron-rich perovskite in the Earth's lower mantle. *Earth Planet. Sci. Lett.* 309, 179–184.
- Mao, Z., Lin, J.F., Yang, J., Wu, J., Watson, H.C., Xiao, Y., Chow, P., Zhao, J., 2014. Spin and valence states of iron in Al-bearing silicate glass at high pressures studied by synchrotron Mössbauer and X-ray emission spectroscopy. *Am. Mineral.* 99, 415–423.
- Mao, Z., Lin, J.-F., Yang, J., Inoue, T., Prakapenka, V., submitted for publication. Effect of the Fe³⁺ spin transition on the equation of state of perovskite.
- Marquardt, H., Speziale, S., Reichmann, H.J., Frost, D.J., Schilling, F.R., Garnero, E.J., 2009. Elastic shear anisotropy of ferropericlase in Earth's lower mantle. *Science* 324, 224–226.
- Masters, G., Laske, G., Bolton, H., Dziewonski, A., 2000. The relative behavior of shear velocity, bulk sound speed, and compressional velocity in the mantle: implication for chemical and thermal structure. In: Karato, S., Stixrude, L., Liebermann, R.C., Masters, G., Forte, A. (Eds.), *Earth's Deep Interior: Mineral Physics and Tomography from the Atomic to the Global Scale*. American Geophysical Union, pp. 63–86.
- McCammon, C., Kantor, I., Narygina, O., Rouquette, J., Ponkratz, U., Sergueev, I., Mezouar, M., Prakapenka, V., Dubrovinsky, L., 2008. Stable intermediate-spin ferrous iron in lower-mantle perovskite. *Nat. Geosci.* 1, 684–687.
- McNamara, A.K., Zhong, S.J., 2005. Thermochemical structures beneath Africa and the Pacific Ocean. *Nature* 437, 1136–1139.
- Murakami, M., Hirose, K., Kawamura, K., Sata, N., Ohishi, Y., 2004. Post-perovskite phase transition in MgSiO₃. *Science* 304, 855–858.
- Murakami, M., Hirose, K., Sata, N., Ohishi, Y., 2005. Post-perovskite phase transition and mineral chemistry in the pyrolytic lowermost mantle. *Geophys. Res. Lett.* 32. <http://dx.doi.org/10.1029/2004gl021956>.
- Murakami, M., Sinogeikin, S.V., Bass, J.D., Sata, N., Ohishi, Y., Hirose, K., 2007a. Sound velocity of MgSiO₃ post-perovskite phase: a constraint on the D'' discontinuity. *Earth Planet. Sci. Lett.* 259, 18–23.
- Murakami, M., Sinogeikin, S.V., Hellwig, H., Bass, J.D., Li, J., 2007b. Sound velocity of MgSiO₃ perovskite to Mbar pressure. *Earth Planet. Sci. Lett.* 256, 47–54.
- Narygina, O.V., Kantor, I.Y., McCammon, C.A., Dubrovinsky, L.S., 2010. Electronic state of Fe²⁺ in (Mg,Fe)(Si,Al)O₃ perovskite and (Mg,Fe)SiO₃ majorite at pressures up to 81 GPa and temperatures up to 800 K. *Phys. Chem. Miner.* 37, 407–415.
- Nishio-Hamane, D., Yagi, T., 2009. Equations of state for postperovskite phases in the MgSiO₃–FeSiO₃–FeAlO₃ system. *Phys. Earth Planet. Inter.* 175, 145–150.
- Oganov, A.R., Ono, S., 2004. Theoretical and experimental evidence for a post-perovskite phase of MgSiO₃ in Earth's D'' layer. *Nature* 430, 445–448.
- Otsuka, K., Karato, S., 2012. Deep penetration of molten iron into the mantle caused by a morphological instability. *Nature* 492, 243–246.
- Panning, M., Romanowicz, B., 2004. Inferences on flow at the base of Earth's mantle based on seismic anisotropy. *Science* 303, 351–353.
- Ringwood, A.E., 1975. *Composition and Petrology of the Earth's Mantle*. McGraw-Hill, New York.
- Sata, N., Shen, G.Y., Rivers, M.L., Sutton, S.R., 2002. Pressure–volume equation of state of the high-pressure B2 phase of NaCl. *Phys. Rev. B* 65. <http://dx.doi.org/10.1103/PhysRevB.65.104114>.
- Shieh, S.R., Dorfman, S.M., Kubo, A., Prakapenka, V.B., Duffy, T.S., 2011. Synthesis and equation of state of post-perovskites in the (Mg,Fe)₃Al₂Si₃O₁₂ system. *Earth Planet. Sci. Lett.* 312, 422–428. <http://dx.doi.org/10.1016/j.epsl.2011.09.054>.
- Shieh, S.R., Duffy, T.S., Kubo, A., Shen, G.Y., Prakapenka, V.B., Sata, N., Hirose, K., Ohishi, Y., 2006. Equation of state of the postperovskite phase synthesized from a natural (Mg,Fe)SiO₃ orthopyroxene. *Proc. Natl. Acad. Sci. USA* 103, 3039–3043.
- Shim, S.H., 2008. The postperovskite transition. *Annu. Rev. Earth Planet. Sci.* 36, 569–599.
- Sidorin, I., Gurnis, M., Helmberger, D.V., 1999. Evidence for a ubiquitous seismic discontinuity at the base of the mantle. *Science* 286, 1326–1331.
- Sinmyo, R., Hirose, K., Nishio-Hamane, D., Seto, Y., Fujino, K., Sata, N., Ohishi, Y., 2008. Partitioning of iron between perovskite/postperovskite and ferropericlase in the lower mantle. *J. Geophys. Res.* 113. <http://dx.doi.org/10.1029/2008jb005730>.
- Sturhahn, W., 2000. CONUSS and PHOENIX: evaluation of nuclear resonant scattering data. *Hyperfine Interact.* 125, 149–172.
- Su, W.J., Dziewonski, A.M., 1997. Simultaneous inversion for 3-D variations in shear and bulk velocity in the mantle. *Phys. Earth Planet. Inter.* 100, 135–156.
- Tateno, S., Hirose, K., Sata, N., Ohishi, Y., 2005. Phase relations in Mg₃Al₂Si₃O₁₂ to 180 GPa: effect of Al on post-perovskite phase transition. *Geophys. Res. Lett.* 32. <http://dx.doi.org/10.1029/2005gl023309>.
- van der Hilst, R.D., de Hoop, M.V., Wang, P., Shim, S.H., Ma, P., Tenorio, L., 2007. Seismotomography and thermal structure of Earth's core–mantle boundary region. *Science* 315, 1813–1817.
- Walter, M.J., Tronnes, R.G., Armstrong, L.S., Lord, O.T., Caldwell, W.A., Clark, S.M., 2006. Subsolidus phase relations and perovskite compressibility in the system MgO–AlO_{1.5}–SiO₂ with implications for Earth's lower mantle. *Earth Planet. Sci. Lett.* 248, 77–89.
- Wen, L.X., Helmberger, D.V., 1998. Ultra-low velocity zones near the core–mantle boundary from broadband PKP precursors. *Science* 279, 1701–1703.
- Wentzcovitch, R.M., Justo, J.F., Wu, Z., da Silva, C.R.S., Yuen, D.A., Kohlstedt, D., 2009. Anomalous compressibility of ferropericlase throughout the iron spin cross-over. *Proc. Natl. Acad. Sci. USA* 106, 8447–8452.
- Wentzcovitch, R.M., Tsuchiya, T., Tsuchiya, J., 2006. MgSiO₃ postperovskite at D'' conditions. *Proc. Natl. Acad. Sci. USA* 103, 543–546.
- Williams, Q., Garnero, E.J., 1996. Seismic evidence for partial melt at the base of Earth's mantle. *Science* 273, 1528–1530.
- Wu, Z.Q., Justo, J.F., Wentzcovitch, R.M., 2013. Elastic anomalies in a spin-crossover system: ferropericlase at lower mantle conditions. *Phys. Rev. Lett.* 110. <http://dx.doi.org/10.1103/PhysRevLett.110.228501>.
- Yu, Y.G.G., Hsu, H., Cococcioni, M., Wentzcovitch, R.M., 2012. Spin states and hyperfine interactions of iron incorporated in MgSiO₃ post-perovskite. *Earth Planet. Sci. Lett.* 331, 1–7.
- Zhang, F.W., Oganov, A.R., 2006. Mechanisms of Al³⁺ incorporation in MgSiO₃ post-perovskite at high pressures. *Earth Planet. Sci. Lett.* 248, 69–76.
- Zhang, L., Meng, Y., Dera, P., Yang, W.G., Mao, W.L., Mao, H.K., 2013. Single-crystal structure determination of (Mg,Fe)SiO₃ postperovskite. *Proc. Natl. Acad. Sci. USA* 110, 6292–6295.